TISSUE REGENERATION

Regenerative potential of prostate luminal cells revealed by single-cell analysis

Wouter R. Karthaus[1]*, Matan Hofree[2]*, Danielle Choi[1], Eliot L. Linton[1], Mesruh Turkekul[7], Alborz Bejnood[2], Brett Carver[1], Anuradha Gopalan[1], Wassim Abida[1], Vincent Laudone[1], Moshe Biton[2], Ojasvi Chaudhary[3], Tianhao Xu[3], Ignas Masilionis[3], Katia Manova[7], Linas Mazutis[3], Dana Pe'er[3,6], Aviv Regev[2,4,5]†, Charles L. Sawyers[1,4]†

Androgen deprivation is the cornerstone of prostate cancer treatment. It results in involution of the normal gland to ~90% of its original size because of the loss of luminal cells. The prostate regenerates when androgen is restored, a process postulated to involve stem cells. Using single-cell RNA sequencing, we identified a rare luminal population in the mouse prostate that expresses stemlike genes (*Sca1*$^+$ and *Psca*$^+$) and a large population of differentiated cells (*Nkx3.1*$^+$, *Pbsn*$^+$). In organoids and in mice, both populations contribute equally to prostate regeneration, partly through androgen-driven expression of growth factors (Nrg2, Rspo3) by mesenchymal cells acting in a paracrine fashion on luminal cells. Analysis of human prostate tissue revealed similar differentiated and stemlike luminal subpopulations that likewise acquire enhanced regenerative potential after androgen ablation. We propose that prostate regeneration is driven by nearly all persisting luminal cells, not just by rare stem cells.

Epithelial tissue homeostasis, at steady state or in response to injury, depends on replenishment of cells by stem cell populations. Whether such stem cells are rare cells with multilineage and self-renewal potential or if they are recruited from lineage-committed cells (facultative stem cells) varies across different tissues (*1*). The normal prostate gland includes luminal epithelial cells, basal epithelial cells, and rare neuroendocrine cells surrounded by stroma and vasculature (*2*, *3*). After surgical or pharmacological castration (a common treatment for advanced prostate cancer), the prostate involutes to ~90% of its original size, mainly because of the loss of luminal epithelial cells (*3*, *4*). Upon exogenous addition of testosterone, the mouse prostate fully regenerates within 4 weeks, which has sparked efforts to identify an underlying stem cell population (*4*–*6*). To provide further insights into this matter, we used single-cell RNA seq (scRNA-seq) to characterize cell types in the murine and human prostate and track their gene expression programs during castration and, in mouse, during regeneration.

[1]Human Oncology and Pathogenesis Program, Memorial Sloan Kettering Cancer Center, New York, NY 10065, USA. [2]Klarman Cell Observatory, Broad Institute of Massachusetts Institute of Technology and Harvard University, Cambridge, MA 02142, USA. [3]Program for Computational and Systems Biology, Sloan Kettering Institute, Memorial Sloan Kettering Cancer Center, New York, NY 10065, USA. [4]Howard Hughes Medical Institute, Chevy Chase, MD 20815, USA. [5]Koch Institute of Integrative Cancer Research, Department of Biology, Massachusetts Institute of Technology, Cambridge, MA 02139, USA. [6]Parker Institute for Cancer Immunotherapy, Memorial Sloan Kettering Cancer Center, New York, NY 10065, USA. [7]Molecular Cytology, Memorial Sloan Kettering Cancer Center, New York, NY 10065, USA.
*These authors contributed equally to this work.
†Corresponding author. Email: aregev@broadinstitute.org (A.R.); sawyersc@mskcc.org (C.L.S)

Results

To characterize the different cell populations of the prostate, we collected droplet-based scRNA-seq profiles from 13,398 cells from the mouse prostate (concentrating initially on the anterior lobe) without fluorescence-activated cell sorting (FACS). We identified 15 distinct cell subsets by unsupervised graph clustering (Fig. 1A and fig. S1, a and b), with further partitioning to 22 subsets, spanning 6 epithelial and 16 nonepithelial subsets (figs. S1, d to f, and S2). To ensure adequate representation of all epithelial cells, we also profiled Epcam-positive and -negative cells isolated by FACS, but found a substantial reduction in quality and near-complete loss of two luminal populations (fig. S1c). We therefore conducted all subsequent experiments using whole mouse prostate anterior lobe without enrichment.

We annotated each of the six epithelial subsets by the expression of marker genes, revealing three seminal vesicle (SV) subsets, a basal subset, and three luminal subsets. The SV subsets (fig. S1e) were defined by two small clusters with high expression of *Pax2*, *Pate4*, and *Calml3*, known epididymal genes that were likely carried over during surgical dissection because of the anatomical proximity of the SV to the prostate lobes. One large subset consisted of basal cells marked by expression of the canonical genes *Trp63*, *Krt5*, and *Krt14* (fig. S1f). Finally, there were three subsets of luminal cells: a large population and two smaller subsets, all three expressing the canonical luminal markers *CD24a*, *Krt8*, and *Krt18* (fig. S1f), labeled as luminal 1 (L1), L2, and L3 cells, respectively.

The nonepithelial subsets revealed a previously unknown complexity in the stromal compartment, specifically the identification of two mesenchymal subpopulations (designated M1 and M2), myofibroblasts and smooth muscle cells. The mesenchymal populations were distinguished by the expression of ligands and/or receptors known to be associated with epithelial growth and differentiation such as *Wnt2*, *Wnt6*, *Wnt10a*, and *RorB* in M1 cells and *Rspo1*, *Fgf10*, and *Sult1e1* in M2 cells (fig. S2b). In addition to M1 and M2, we identified myofibroblasts and smooth muscle populations on the basis of the expression of canonical contractile genes such as *Acta2* and *MyH11*. These cells separately expressed *Rspo3* or *Notch3* (fig. S2e), revealing a level of complexity greater than that suggested previously (*7*). All of these populations expressed the gene encoding the androgen receptor, suggestive of hormone-driven communication with epithelial cells (discussed below). We also identified multiple immune populations, such as B and T lymphocytes, natural killer (NK) cells, dendritic cells (*Xcr1*), and four subpopulations of monocytes and macrophages (*CD14*, *IBA1*). Other cell types included vascular endothelial cells (*CD31*), lymphatic endothelial cells (*CD31*, *Prox1*), and glial cells (*Sox10*) (fig. S2, b and c). We did not observe a distinct neuroendocrine cluster, most likely because of the rarity of neuroendocrine cells (fig. S2d).

Of the three luminal subpopulations, L1 cells were predominant (~96% of profiled luminal cells) and expressed high levels of canonical androgen receptor target genes such as *Pbsn* and *Nkx3.1*, as well as *CD26/Dpp4*, *CD59a*, and *CD133/Prom1* (Fig. 1B and fig. S3, a and b). Although L1 cells form a single subset using unsupervised graph clustering (t-distributed stochastic neighbor embedding, tSNE), there is variation within the subset as revealed by hierarchical clustering of differentially expressed genes (fig S3d). By contrast, L2 (~3%) and L3 (1%) are distinct minority luminal populations. L2 cells express *Sca1/Ly6a*, *Tacstd2/Trop2*, and *Psca*, all of which have been previously associated with stem cell–like activity, as well as *Krt4* and Claudin10 (Fig. 1B and fig. S3, a, b, and h). L3 cells are defined by expression of the transcription factor *Foxi1*, a master regulator of subunits of the vacuolar ATPase proton pump such as *Atp6v1g3* and *Atp6b1b* (*8*), both of which are strongly expressed in these cells (Fig. 1B and fig. S3, a and b). We and others have recently identified Foxi1$^+$ pulmonary ionocytes with features similar to those of cells in the gills of freshwater fish that regulate ion transport. Pulmonary ionocytes regulate salt balance in airway secretions and may be implicated in the pathophysiology of cystic fibrosis (*9*, *10*). We also detected *Foxi1*-expressing cells among

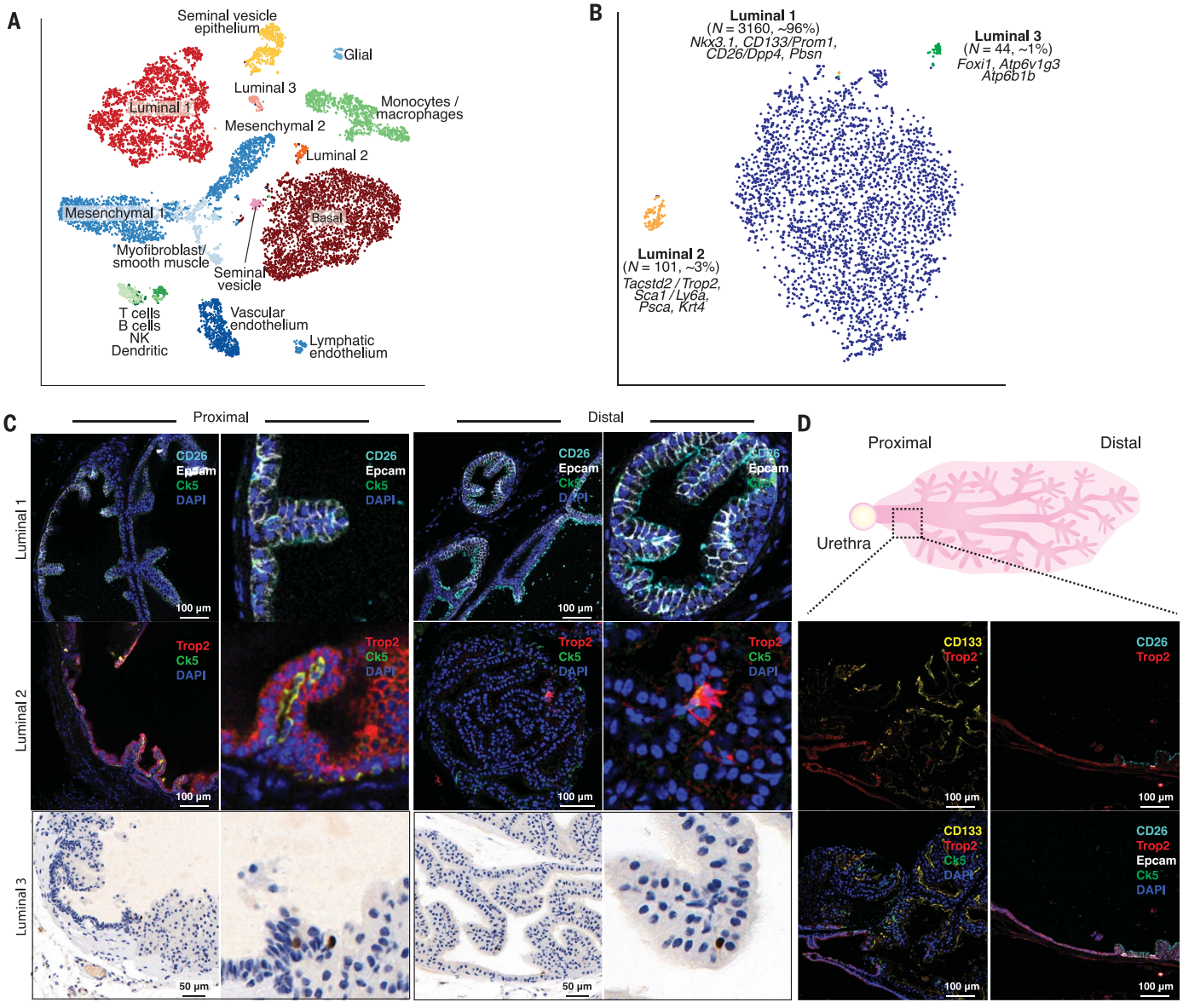

Fig. 1. Three subsets of luminal cells identified by scRNA-seq of the intact mouse prostate. (**A**) Single-cell census of the intact prostate. Shown is tSNE of scRNA-seq profiles colored by unsupervised clustering of 15 subsets and labeled post hoc. (**B**) Prostatic luminal subtypes. Shown is tSNE of scRNA-seq profiles only from the luminal clusters in (A). (**C**) Validation of luminal subset markers in situ. Shown is immunofluorescence (IF) staining of L1 (CD26/Dpp4, cyan, top) and L2 (Tacstd2/Trop2, red, middle) markers in the proximal and distal anterior lobe, along with Epcam (for epithelial cells, white), Ck5 (basal cells, green), and DAPI (nuclei). Also shown is IHC staining of Foxi1 in the proximal and distal anterior lobe (bottom). (**D**) Sharp transition from L2 to L1 cells. Shown is IF staining of L1 (CD133/Prom1 or CD26/Dpp4) and L2 (Tacst2/Trop2) markers, along with Epcam (for epithelial cells), Ck5 (basal cells), and DAPI (nuclei). A distinct border can be observed between proximal and distal prostatic regions. Scale bars, 100 or 50 µm as labeled.

the *Pax2*$^+$ SV population (fig. S3a). Male *Foxi1*-null mice are infertile because of a failure to properly acidify the epididymal fluid (*11*).

In situ analysis revealed that L1 cells (CD26/Dpp4$^+$CD133/Prom1$^+$) are almost exclusively found in the distal prostate ducts, whereas L2 cells (Trop2$^+$) are predominantly located in the proximal prostate (Fig. 1C and fig. S3, e to h), a pattern consistent with prior studies of Psca$^+$ or Sca1/Ly6a$^+$ cells (*12*, *13*). The spatial transition from L2 to L1 cells is abrupt when moving distally along a proximal duct (Fig. 1D), suggesting that anatomically localized inductive signals have a role in defining L1 versus L2 cell fates. By contrast, ionocyte-like L3 cells are interspersed in both proximal and distal locations (Fig. 1C). The in situ pattern for L1, L2, and L3 cells was similar in the dorsolateral prostate but not in the ventral prostate, where we observed an expanded number of Trop2$^+$ and Claudin10$^+$ L2 cells, indicative of variability in the relative percentage of L1 and L2 cells in different lobes (fig. S4).

Gene expression changes in the mouse prostate across a castration/regeneration cycle

Because the murine prostate gland can fully regenerate after castration-induced involution, there has been considerable interest in defining potential stem cells underlying this regeneration. Although a fraction of luminal cells is known to persist after castration (*14*, *15*), little is known about their transcriptional features relative to those in hormonally intact mice. The small fraction of L2 cells (~3%) relative to L1 cells, together with prior data

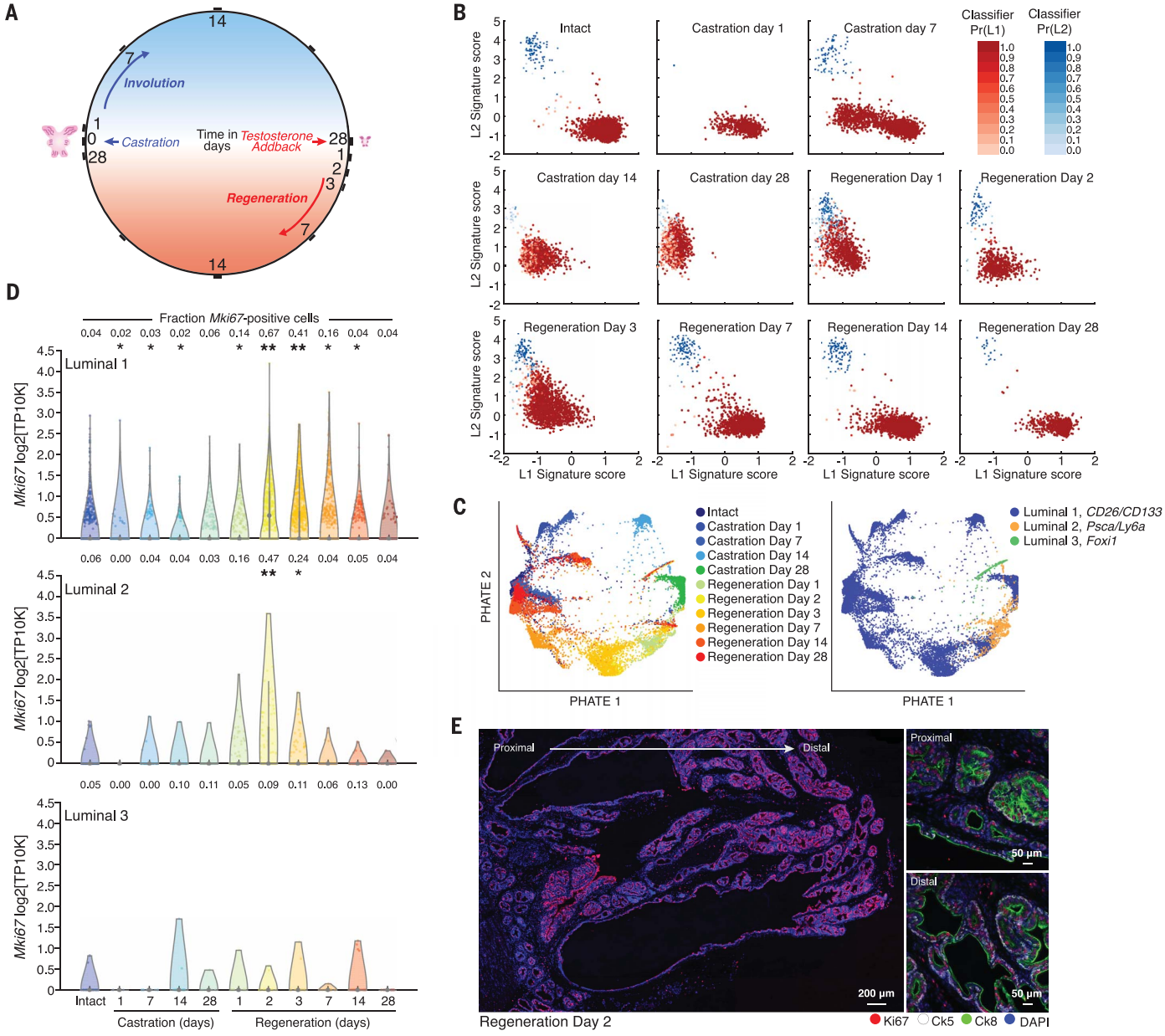

Fig. 2. Transcriptomic changes in murine luminal subpopulations during castration and organ regeneration. (**A**) Schematic overview of the C/R cycle with experimental time points. (**B**) Scatterplots of the L1 (*x* axis) and L2 (*y* axis) intact signature score (*z* score) for each cell (dot) assigned to L1 (red) or L2 (blue) at each time point (panel). Dot color intensity is scaled by the strength of classifier assignment probability for the dot's assigned class (color bar). (**C**) Similar transcriptional states of L1 and L2 during castration. PHATE graph of scRNA-seq profiles from luminal cells, colored by time point (left panel) or L1, L2, and L3 based on expression profiles in T0 (right panel). L1 cells undergo the most substantial transcriptional changes. On castration day 28 (dark green, left panel) and regeneration day 1 (light green, left panel) L1 are coembedded with L2 cells (orange, right panel). (**D**) Rapid entry of L1 and L2 cells into the cell cycle during regeneration. Each plot shows the distribution of *Mki67* mRNA expression (*y* axis) throughout the C/R cycle (*x* axis) for L1, L2, and L3 cells. Fraction of cells with *Mki67* expression detected is noted on top. *Expression is significantly different from intact (T0) (Bonferroni-corrected $P < 0.05$, one-sided Wilcoxon rank-sum test). **Fold change of 1.5 or greater and area under the curve of 0.65. (**E**) IF staining of Ki67 in the anterior lobe at regeneration day 2. (Left) Low-magnification image showing proximal and distal regions. (Right) representative higher magnification (20×) of proximal and distal regions. Shown are Ki67 (red), Ck8 (Green), Ck5 (white), and DAPI (purple). Scale bars, 200 or 50 µm as labeled.

implicating the L2-expressed genes *Sca1/Ly6a*, *Psca*, and *Tacstd2/Trop2* as prostate stem cell markers (*13*, *16*), prompted us to investigate whether L2 cells function as stem cells in regeneration.

To this end, we collected scRNA-seq profiles of the mouse prostate throughout a complete castration/regeneration (C/R) cycle (Fig. 2A and fig. S5, a and b). We first compared the relative frequency of L1 and L2 cells in castrated mice using FACS with cell surface markers that distinguish between L1 (CD26/Dpp4 or CD133/Prom1) and L2 (Sca1/Ly6a) cells. L2 cells were two- to threefold enriched in castrated versus intact mice, consistent with a potential stem cell role (*12*); however, the majority (>50%) of persistent luminal cells ($CD24^+$; $CD49f^-$) were L1 ($CD26/Dpp4^+$; $CD133/Prom1^+$) (fig. S5, c to e). Computational analysis of transcriptomes across the C/R cycle revealed, on the basis of

scatterplots of L1 versus L2 signature scores, that L1 cells gain features very similar to L2 cells after castration (day 28) but revert back to baseline during regeneration (Fig. 2B and fig. S6c). This result was seen using both raw and scaled classification scores (fig. S6d) and was further supported by pairwise correlation of L1 and L2 expression profiles, which peaked on day 28 after castration and then declined during regeneration (fig. S6b). In addition, hierarchical clustering based on program genes showed that L1 and L2 cells co-cluster 28 days after castration and 1 day into regeneration but not at other time points (fig. S7). By contrast, L3 cells remained distinct from L1 and L2 throughout this cycle despite robust androgen receptor expression ($P < 0.05$, Wilcoxon rank-sum test) (fig. S6, b to d). Finally, when visualized by PHATE (*17*), a graph diffusion–based 2D embedding approach that preserves global distance relationships, transcriptional profiles of L1 and L2 cells were closely embedded on day 28 after castration but separated by day 28 after regeneration (Fig. 2C and fig. S6a). Similar co-embedding was also observed with other dimensionality reduction methods (fig. S5b). One reason for the similarity in transcriptional features of L1 and L2 cells after castration is loss of androgen receptor–regulated transcription, which contributes substantially to the distinction between these two populations in the presence of androgen. For example, there is a substantial decline in the expression of *CD59a* and *Nkx3.1* in L1 cells and of *Psca* in L2 cells. Conversely, genes whose transcription is not dependent on the androgen receptor, such as *CD26/Dpp4* and *Sca1/Ly6a*, maintain L1- and L2-specific expression (fig. S8b), indicating that the two populations remain distinct.

Enhanced regenerative potential of luminal cells in mouse organoid culture

In light of the overlapping transcriptomic features of L1 and L2 cells after castration, we explored the relative contribution of each to regeneration, starting with an analysis of their recruitment into the cell cycle after androgen (testosterone) addback. Sixty-eight percent of L1 cells and 45% of L2 cells had a surge in *Ki67* transcript expression (a marker of proliferating cells) just 2 days after implantation of testosterone pellets; in addition, there was increased expression of G_1/S and G_2/M cell cycle gene sets ($P < 0.05$, Wilcoxon rank-sum test) (Fig. 2D and fig. S5, f and g). These findings were confirmed in situ, on the basis of robust Ki67 staining throughout the prostate, 2 to 3 days after androgen addback, particularly in the distal gland where L1 cells reside (Fig. 2E and fig. S9). L3 cells and basal epithelial cells also showed increased *Mki67* expression but at more modest levels (11 and 15%, respectively; $P < 0.05$, Wilcoxon rank-sum test) (Fig. 2D and fig. S5h).

The fact that so many luminal cells rapidly enter the cell cycle during the C/R cycle suggested to us that a larger number of persisting cells might contribute to regeneration than would be predicted from a conventional stem cell model. As a first test of this hypothesis, we measured the organoid regeneration potential of a pan-luminal epithelial cell population ($CD24^+$, $CD49f^-$) from castrated mice and from mice after 1, 2, or 3 days of androgen addback. We observed an increase in the efficiency of organoid formation from ~5 to >20% within 2 days (fig. S10a). To dissect the relative roles of L1 and L2 cells in this regeneration, we isolated L1 cells ($CD26/Dpp4^+$ or $CD133/Prom1^+$) and L2 cells ($Sca1/Ly6a^+$) at different time points along the C/R cycle and compared their organoid formation potential. L2 cells from intact mice showed superior organoid formation (9 to 10%) compared with L1 cells (~4%) ($P < 0.05$, *t* test) (Fig. 3A), as expected from prior studies of $Sca1/Ly6a^+$ cells (*12*). However, L1 cells generated twofold more organoids in the castration setting (~9%; $P < 0.05$, *t* test), with a further doubling (~20%) 2 days into regeneration ($P < 0.05$, *t* test) (Fig. 3, A and B, and fig. S10, b and c). L2 cells also generated more organoids 2 days after regeneration (Fig. 3B) but the change after castration was not significant (Fig. 3A). In addition, both L1- and L2-derived organoids gave rise to $Ck5^+$ basal cells (Fig. 3C and fig. S10d), indicative of their bilineage potential. L1-derived organoids also displayed more polarized morphology and thicker walls, consistent with their more differentiated gene expression profile in hormonally intact glands (Fig. 3C and fig. S10d). Regeneration potential was not influenced by dihydrotestosterone (DHT) in the organoid culture medium ($P > 0.05$, *t* test) (Fig. 3B) despite robust androgen receptor expression in L1 and L2 cells. This result suggests that the effect of in vivo testosterone supplementation on luminal cell regeneration is indirect, which we address further below.

Lineage tracing of luminal cells during murine prostate regeneration

To determine the contribution of persisting luminal cells to prostate regeneration in vivo, we conducted a lineage-tracing experiment by crossing the Rosa26/four-color Confetti allele (*18*) with the luminal-specific *Krt8* Cre^{ERT2} driver (*19*) (Fig. 3D). In contrast to prior lineage-tracing experiments using a prostate-specific antigen Cre driver (*20*), *Krt8* expression was robust in luminal cells after castration, as shown by successful marking of single luminal cells throughout the prostate (~6%) 1 week after injecting mice with tamoxifen (Fig. 3E, fig. S11a, and tables S1 and S2a). We were unable to identify any labeled basal cells (3 mice, $n = 1204$ cells), indicative of the specificity of the K8-Cre driver for luminal cells (table S1a and fig. S11b). To determine the relative contribution of labeled cells to regeneration, we examined fully reconstituted prostate glands 4 weeks after androgen addback. Analysis of ~450 clones from each of three independent mice revealed an average clone size of ~4.5 cells (4.40 ± 0.39, 95% confidence intervals), indicative of two to three doublings per cell. The different clones were distributed throughout the proximal and distal regions of individual prostate ducts, suggesting that they each arose locally rather than by migration from proximal "stemlike" cells (Fig. 3, E and F; fig. S11, c to e; and table S2). Moreover, the number of labeled luminal cells remained constant (~6%) after 28 days (table S6a), suggesting that they contribute uniformly to the regenerated gland. Proximal clones were slightly smaller (3.47 ± 0.21 cells) than the overall clone size (4.4 ± 0.35 cells; $P < 0.05$, Welch's *t* test) (table S5b). In situ analysis using L1 (CD26/Dpp4)– and L2 (Tacstd2/Trop2)–specific markers revealed that most clones (located distally) were composed of L1 cells, whereas proximal clones were composed exclusively of L2 cells. Rare $Ck5^+$ basal cells were detected in some clones (<1% tracing events) (table S1c), indicating that luminal cells retain bilineage potential during regeneration (fig. S11c).

Mesenchymal-derived growth factors support luminal cell growth in organoid culture

To explain the discrepancy between the effects of androgen addback in vivo (which greatly enhanced the clonogenicity of L1 cells in organoid culture) versus androgen supplementation in vitro (which had no effect), we postulated that the effect of in vivo androgen addback is indirect despite robust androgen receptor expression in L1 cells. Indeed, early work using renal capsule tissue recombination assays reported an essential role of androgen receptor in mesenchymal cells in prostate regeneration, demonstrating the importance of androgen-regulated mesenchymal growth factors (*21*). More recent studies of conditional *Ar* deletion have shown that the androgen receptor is dispensable for luminal regeneration after castration but is required for certain functions such as proliferation of castration-resistant, Nkx3.1-expressing luminal cells (*22*).

To address this discrepancy, we examined the effect of in vivo androgen addback on non-epithelial cells and observed profound transcriptional changes in M1 and M2 mesenchymal subpopulations during the C/R cycle (fig. S12, a and b), which were similar in extent to the changes seen in luminal cells (Fig. 2C) and basal cells (fig. S12b). We reasoned that reciprocal changes in the levels of ligands and/or cognate receptors may provide clues to cell-cell circuits

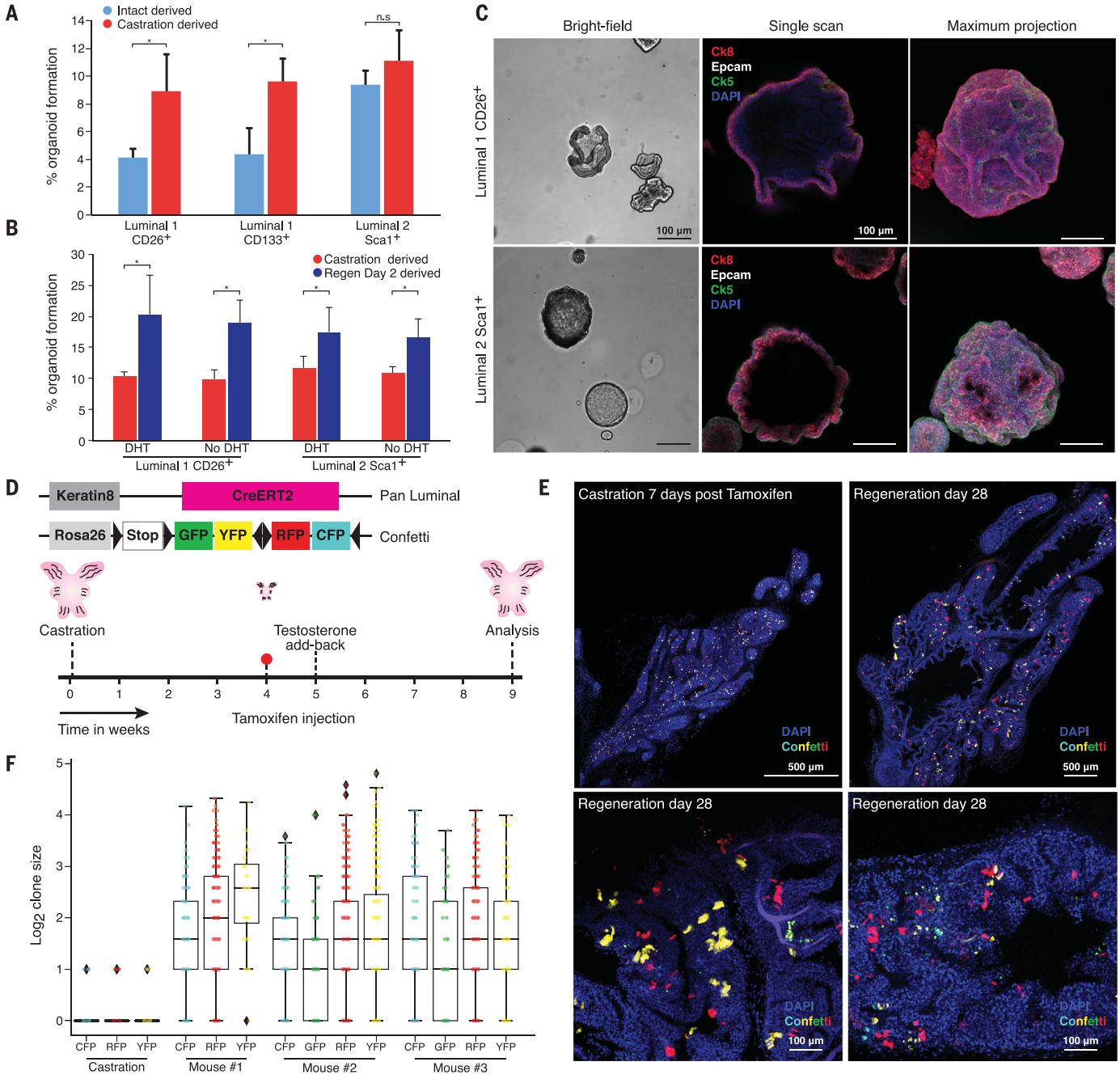

Fig. 3. Enhanced regenerative potential of murine luminal cells after castration in organoid culture and in vivo. (**A** to **C**) Enhanced organoid formation of L1 and L2 cells isolated after castration or during regeneration. (A) Relative organoid formation (%, *y* axis; mean ± SD) in the presence of 1 nM DHT in cultures initiated by L1 or L2 cells isolated by CD26/Dpp4 (L1), CD133/Prom1 (L1), or Sca1/Ly6a (L2) expression from hormonally intact prostate (blue) or prostate 28 days after castration (red). The number of organoids was quantified 7 days after seeding 200 cells ($N = 3$; $^*P < 0.05$, *t* test). (B) Relative organoid formation (%, *y* axis; mean ± SD) from L1 or L2 cells isolated by CD26/Dpp4 or Sca1/Ly6a expression, respectively, from a prostate 28 days after castration (red) or a prostate 2 days into regeneration (blue) in the presence or absence of 1 nM DHT. The number of organoids was quantified 7 days after seeding 200 cells ($N = 3$; $^*P < 0.05$, *t* test). (C) Representative images of organoids derived from CD26/Dpp4$^+$ L1 cells (top) or Sca1$^+$ L2 cells (bottom). (Left) Bright-field images. (Right) Confocal images (single *Z* and maximum projection) stained with Ck8 (red) or Ck5 (green), Epcam (white), or DAPI (purple) 7 days after establishment. Scale bars, 100 µm. (**D**) Lineage-tracing strategy. (**E** and **F**) Contribution of multiple clones to prostate gland regeneration. (E) (Top) Maximum projection of a castrated prostate 7 days after tamoxifen injection (left) and 4 weeks after regeneration (right). Only red fluorescence protein (RFP) and yellow fluorescence protein (YFP) are shown. Scale bars, 500 µm. (E) (Bottom) Higher magnification of lineage-traced prostates showing contribution of multiple clones to gland regeneration. Scale bars, 100 µm. (F) Distribution of size of different color clones. Log_2 clone size (*y* axis) is plotted from three independent mice compared with control (castrated 7 days after tamoxifen) (*x* axis). Raw data are shown in table S2. As observed previously, GFP$^+$ clones are infrequent in the prostate (*34*).

that drive prostate regeneration. We thus searched for changes in androgen-dependent expression of previously annotated ligand-receptor pairs (*23*) across the complete C/R cycle in all cells in the prostate. Between every pair of cell subtypes (e.g., L1 and M2), we tested the enrichment of ligand-receptor pairs that were differentially expressed across the subtypes (table S3). Among the most substantial changes in ligand expression at the mRNA level were neuregulin 2 (*Nrg2*) (M1 and smooth muscle 1), insulin-like growth factor 1 (*Igf1*) (M1 and M2), fibroblast growth factor 10 (*Fgf10*) (M2), and r-spondin 3 (*Rspo3*) (smooth muscle 1) (Fig. 4A and fig. S12c), with corresponding changes in fibroblast growth factor receptor 2 (*Fgfr2*) and leucine-rich repeat containing G protein–coupled receptor 4 (*Lgr4*) expression, primarily in L1 cells. All of these signaling pathways are implicated in prostate development (*24*–*27*). We also observed a modest increase in epidermal growth factor (*Egf*) ligand expression by L1 cells within 24 hours of androgen addback that peaked after full reconstitution. This is noteworthy because EGF is a key component of epithelial organoid culture media (Fig. 4A and fig. S12c). We confirmed the spatiotemporal expression of these growth factors in situ during the C/R cycle using RNA fluorescence in situ hybridization (RNA-FISH) (Fig. 4B and fig. S13).

To test the functional impact of these mRNA expression changes, we compared the organoid generation potential of L1 and L2 cells isolated from castrated mice in standard medium (with EGF, Noggin, R-spondin, and A83) with new media conditions guided by the growth factor expression changes identified by single-cell analysis (Fig. 4C and fig. S14a). Nrg stimulated growth 10-fold in L1 cells and fivefold in L2 cells, even when androgen receptor signaling was pharmacologically inhibited

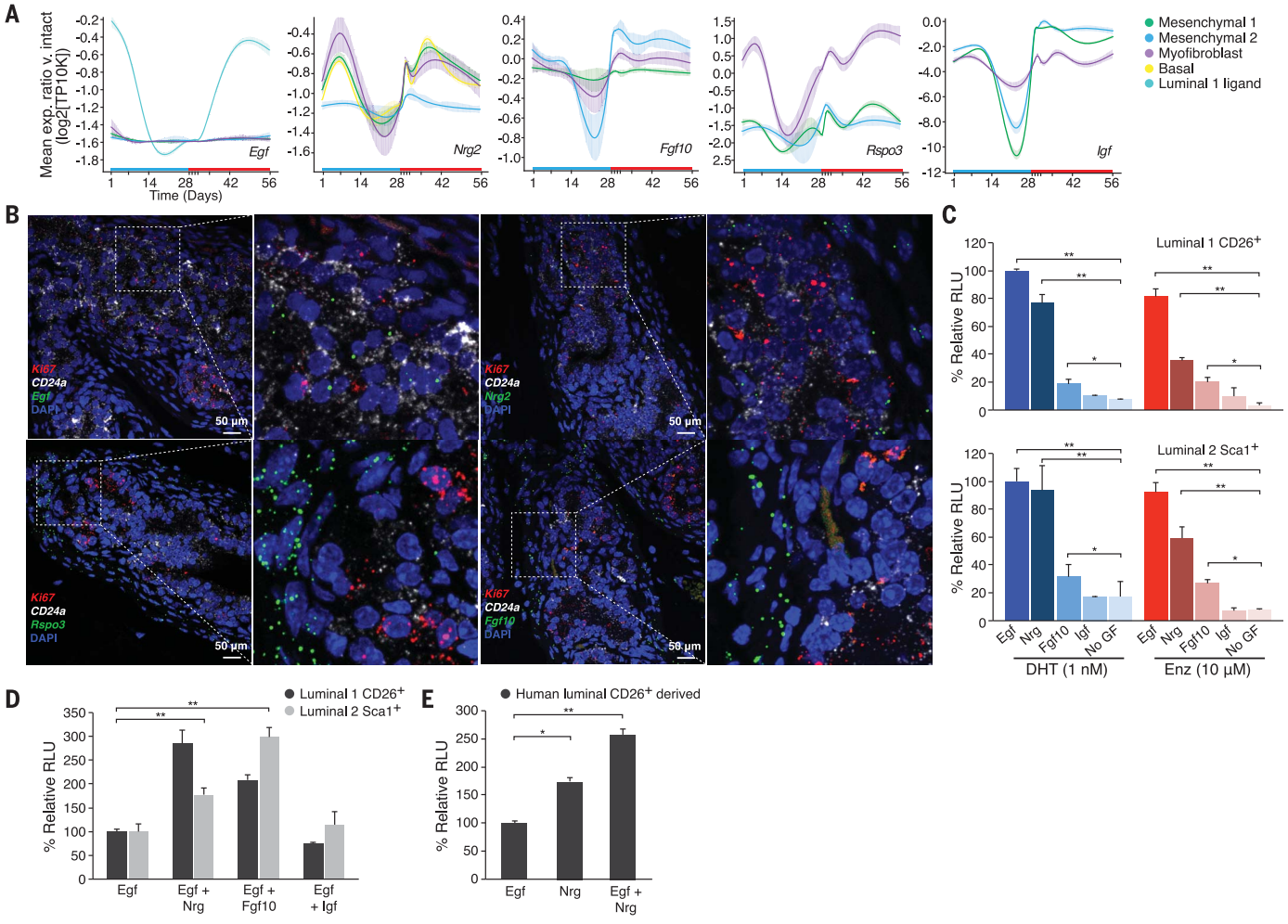

Fig. 4. Androgen receptor–mediated induction of neuregulin in mesenchymal cells is a potential driver of luminal regeneration. (**A**) Changes in expression of key stromal ligands over the C/R time course. Shown is the smoothed mean expression relative to intact prostate (T0) (*y* axis) of ligands in different subsets of stromal and epithelial cells (per color code). (**B**) In situ validation of growth factor expression by RNA-FISH of prostate tissue isolated on regeneration day 2. Representative growth factors (*Egf*, *Nrg2*, *Rspo3*, and *Fgf10*; green), luminal cells (*CD24a*; white), and proliferating cells (*Mki67*; red) are shown. Scale bar, 25 µm. (**C** to **E**) Nrg promotes luminal regeneration in mouse and human organoids. (C) Relative proliferation of murine L1 cells (CD26/Dpp4$^+$; top) and L2 cells (Sca1/Ly6a$^+$; bottom) in the presence of Egf, Nrg, Fgf10, Igf, or no growth factor in the presence of DHT (1 nM) or enzalutamide (10 µM). The data are displayed as average growth ± SD (*y* axis) of 5000 cells measured by CellTiter-Glo at 7 days. Base organoid medium contains noggin, R-spondin, A83-001, and Y-27632. $N = 3$. $^*P < 0.05$, $^{**}P < 0.01$, *t* test. (D) Relative proliferation of murine L1 and L2 cells measured as in (C) in the presence of EGF alone or EGR in combination with Nrg, Ffg10, or Igf, all in the presence of DHT (1 nM) (*x* axis). $N = 3$. $^*P < 0.05$, $^{**}P < 0.01$, *t* test. (E) Relative proliferation of human prostate luminal cells (CD26/DPP4$^+$) measured as in (C) in the presence of EGF, NRG, or ERG plus NRG in base human organoid medium (NOGGIN, R-SPONDIN1, FGF2, FGF10, PGE2, A83-001, NICOTINAMID, SB202190, DHT, and Y-27632). $N = 3$. $^*P < 0.05$, $^{**}P < 0.01$, *t* test. Human organoids for this panel were derived from normal prostate tissue isolated during cystectomy surgery.

by enzalutamide. Histologically, Nrg-treated organoids had larger lumens with more polarized luminal cells, a phenotype that was inhibited by enzalutamide (figs. S12e and S14b). Fgf10 had a more modest effect on growth (twofold over background), whereas Igf1 was inactive (Fig. 4C and figs. S12e and S14a). Combinations of Erg$^+$Nrg or Egf$^+$Fgf10 stimulated growth and lumen size even more potently, at levels two- to threefold above those seen with Egf alone (Fig. 4D and figs. S12f and S14c). These growth factors were similarly

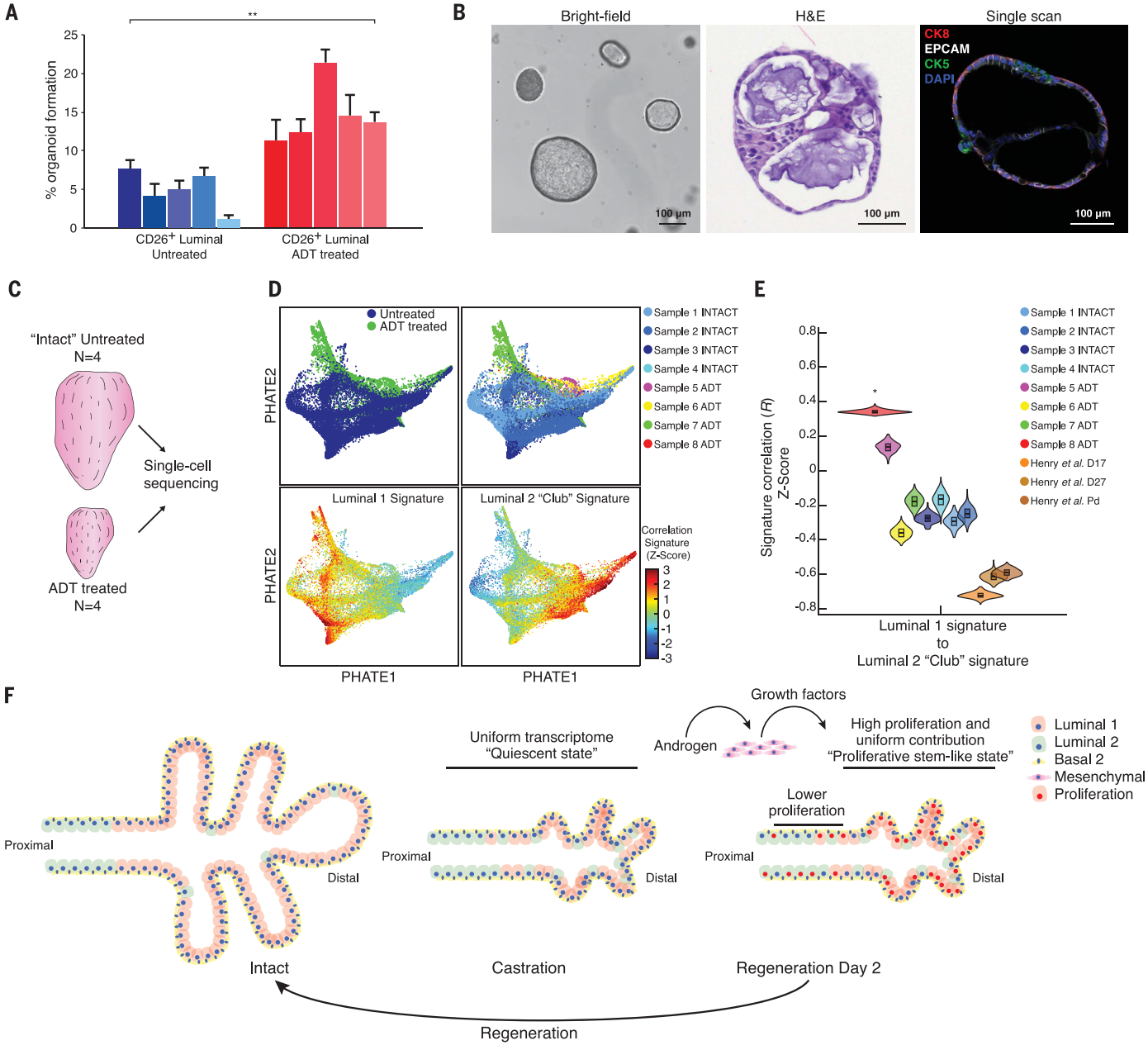

Fig. 5. Androgen deprivation enhances the regenerative potential of human prostate luminal cells. (**A**) Enhanced organoid formation by human luminal cells obtained after castration. (Left) Relative organoid formation (mean ± SD) of CD26/DPP4$^+$ luminal cells isolated from prostates obtained by radical prostatectomy from hormonally intact patients (N = 5, blue) or patients treated with androgen deprivation therapy (N = 5, red). Organoids were quantified 14 days after seeding of 200 cells. N = 4. $^{**}P < 0.01$, Welch's t test. (**B**) Representative bright-field image (right), H&E-stained image (middle), and confocal image (right) of a human organoid derived a patient treated with ADT as in (A). For the confocal image: CK8 (red), CK5 (green), EPCAM (white), and DAPI (purple). Scale bar, 100 µm. (**C**) Schematic of human prostate processing for scRNA-seq. (**D**) (Top) PHATE map of luminal cells from all samples stratified by treatment (left) and by sample (right). (Bottom) PHATE maps colored by correlation to RNA signatures derived from Henry *et. al.* (*30*). Shown are L1 cells (left) and L2 "Club" cells (right). (**E**) Pairwise correlation of signature scores for L1 and L2 "Club" cells (*30*) per patient after CNA filtering. Signatures were generated using previously published human prostate luminal cell data (*30*). *Significant change of the median correlation ($P < 0.05$, Welch's t test, one-sided test). (**F**) Model of prostate regeneration. The prostate gland shrinks ~90% after androgen deprivation (castration) because of the loss of luminal epithelial cells. During this process, the transcriptome of L1 cells closely resembles that of more stemlike L2 cells. Androgen addback stimulates production of growth factors by distinct populations of mesenchymal cells, which rapidly recruit nearly all persisting luminal cells into the cell cycle. Each of these proliferating luminal cells collectively contributes to the regeneration of the prostate gland, rather than a rare stem cell population.

active in promoting the growth of normal human prostate organoids, indicative of cross-species conservation (Fig. 4E and figs. S12, g and h, and S14, d and e).

Luminal subpopulations are present in human prostate, with enhanced regenerative properties after androgen ablation

To determine whether the castration-induced changes in the regenerative potential of murine luminal cells extends to human prostate, we isolated luminal populations from prostate samples derived from men who were treated for prostate cancer by radical prostatectomy after receiving androgen deprivation therapy (ADT) (fig. S15a). We focused specifically on histologically normal regions to minimize contamination with tumor cells. As controls, we isolated luminal cells samples from five hormonally intact prostate cancer patients treated with radical prostatectomy. CD26/DPP4$^+$ cells isolated from ADT-treated patients displayed a threefold increase in organoid formation (14.6 ± 3.9%) compared with those from the hormonally intact patients (4.9 ± 2.5%) ($P < 0.05$, Welch's t test) (Fig. 5A and fig. S15b), consistent with our findings in mice. Moreover, these CD26/DPP4$^+$ cells could give rise to PSCA$^+$ luminal cells and CK5$^+$ basal cells, indicative of their multipotency in vitro (Fig. 5B and fig. S15c).

To determine the effect of androgen withdrawal on RNA expression in the human prostate, we generated scRNA-seq profiles from the histologically normal regions of eight of these samples (four hormonally intact and four ADT treated) (Fig. 5C). To ensure that our analysis was restricted to normal cells (and not tumor cells), we inferred single-cell DNA copy number alteration (CNA) profiles on the basis of expression of genes from large genomic regions (*28*). CNAs typical of those seen in primary prostate cancer, such as 3p14, 8p, 8q, 13q, and 16q (*29*), were faithfully identified by inferCNV in luminal cells from samples with histologically confirmed tumor cells (e.g., intact sample 2 and ADT sample 3) (figs. S16 and S17). However, cells with predicted CNAs consistent with known prostate cancer alterations were also detected in histologically normal regions at frequencies ranging from 17 to 50% of luminal cells in the hormonally intact patients. Although some of these cells clustered by their expression profiles with their copy-neutral counterparts (fig. S18) and therefore may be false positives, we conservatively filtered all CNA-predicted cells from all subsequent analyses to ensure that we focused on normal prostate cells.

Unsupervised clustering defined 20 cell subsets in the hormonally intact prostate. Reminiscent of the murine prostate, B cell, T cell, NK cell, macrophage, and dendritic cell populations were present in all samples (fig. S19a). The stromal compartment contained vascular and lymphatic endothelium, glia, and two distinct smooth muscle and mesenchymal populations expressing *WNT2*, *FGF10*, or *RSPO3* (fig. S20). We identified four distinct epithelial clusters (two basal and two luminal) and one small neuroendocrine cluster (fig. S19, b to d). The two basal cell clusters share expression of the canonical basal markers *KRT5*$^+$and *TP63*$^+$ and are primarily distinguished by the expression of *KRT13*$^+$. Basal cells expressing *KRT13*$^+$ have previously been observed in the lung trachea in specific histological structures called "hillocks" (*9*, *30*). The larger luminal population shares features with L1 cells in the mouse, such as expression of secretory and AR-regulated genes (*CD26/DPP4*^{high}, *KLK3/PSA*^{high}, and *PLA2G2A*$^+$). The smaller luminal population is more stem like (*PSCA*$^+$ and *KRT4*$^+$), reminiscent of L2 cells in the mouse, and is primarily distinguished by expression of the secretoglobulin family gene *SCGB1A1*$^+$. Murine *Scgb1a1* is a marker of club cells, a subpopulation in the lung with long-term repopulating activity (*31*, *32*) (Fig. 5D and figs. S19b, S21, and S22). Luminal cells expressing both L1 (*PLA2G2A*^{low}) and L2 (*PSCA*) markers were detected in some samples (figs. S19b and S21). These are unlikely to be doublets from coencapsulation or incomplete digestion because of their relatively high abundance and the fact that L1 and L2 cells are spatially distinct. Their presence thus suggests the possibility of bipotent progenitor cells or cells in transition, which we label luminal intermediates (fig. S21). Although we did not identify a distinct human luminal 3 (ionocyte) cluster by scRNA-seq, we observed rare FOXI1$^+$ cells interspersed throughout the gland using immunohistochemistry (IHC) (fig. S19d). To determine whether the human counterparts of mouse L1 and L2 cells also share transcriptional features after androgen withdrawal, we compared their expression profiles in hormonally intact and ADT samples. Signatures of human L1 and L2 cells from two of the ADT samples (samples 5 and 8) showed evidence of coembedding in either tSNE or a PHATE map and had a higher correlation of L1 and L2 profiles compared with intact samples (Fig. 5, D and E, and figs. S23, a to c, and S24). One of the ADT samples where L1 and L2 cells did not show this enhancement in shared features had significant tumor content (~50% by histology, Gleason grade 9) despite our attempts at filtering by inferred CNA profiles (fig. S23, d to f).

Discussion

Our study has uncovered a previously unknown complexity of cell subtypes within the prostate. In addition, we found that after castration, most persisting luminal cells (rather than a rare population of stem cells) contribute to the proliferative response, akin to the regenerative process observed after liver injury (*33*). In hormonally intact mice, the prostate gland contains three primary luminal subtypes, the most predominant of which are the secretory epithelial cells lining the distal branching ducts, which we call L1 or secretory luminal cells. Murine L2 cells (*Sca1/Ly6a*$^+$, *Psca*$^+$, and *Tacstd2/Trop2*$^+$) have been described previously in independent reports examining the expression of each of these markers, but our work now consolidates this into a single subtype. Anatomically, L2 cells line the proximal duct with a very sharp transition to L1 cells in distal branching ducts, suggestive of a hierarchical relationship during prostate development. In humans, the L2 counterpart is primarily defined by the club cell marker *SCGB1A1*$^+$; in the lung, cells with this marker are responsible for airway maintenance (*31*). L3 cells have not been previously identified but they resemble pulmonary ionocytes, which have been implicated in the regulation of salt balance within airways (*9*, *10*). Analogous luminal subpopulations are present in humans, with the caveat that L3 cells were detected by IHC only.

An important question is what is the mechanism by which persisting luminal cells acquire enhanced self-renewal, particularly because L1 cells are well-differentiated secretory cells at baseline. The fact that L1 and L2 cells acquire stemlike transcriptional features in response to castration suggests a reprogramming event or cell state change. This hypothesis is further supported by androgen-regulated expression of known stem cell niche factors (Nrg, Fgf10, and Rspo3) in mesenchymal cells. Although we cannot rule out the possibility that a subset of cells with preexisting self-renewal properties is present within the hormonally intact gland, our transcriptomic analysis failed to define a distinct subpopulation matching that of persistent L1 cells (fig. S6e).

Although we have not yet directly explored the implications of these luminal cell subtypes in cancer, it is noteworthy that mice with *Nkx3.1*- and *CD133/Prom1*-specific Cre expression (each of which is L1 restricted) develop prostate cancers when crossed with various floxed cancer driver alleles (*34*, *35*). Thus, L1 cells can clearly serve as cells of origin for prostate cancer. It will be of interest to explore this question with L2-specific Cre drivers (e.g., *Psca*), as well as in L3 cells. Another question is whether the persistence of large numbers of luminal cells after castration has clinical relevance, particularly for the use of ADT in prostate cancer patients. A precise molecular understanding of how differentiated normal luminal cells acquire stemlike regenerative properties could provide insight into ways to interfere with this

process in malignant prostate cells. Our work suggests that microenvironmental niche factors such as NRG and FGF10 may play a role. Because cancer cells often exploit the stemlike niches used by normal cells, these insights could suggest new prostate cancer therapies that might be useful in combination with AR blockade.

REFERENCES AND NOTES

1. H. Clevers, F. M. Watt, *Annu. Rev. Biochem.* **87**, 1015–1027 (2018).
2. J. E. McNeal, *Am. J. Surg. Pathol.* **12**, 619–633 (1988).
3. H. F. English, N. Kyprianou, J. T. Isaacs, *Prostate* **15**, 233–250 (1989).
4. X. Wang *et al.*, *Nature* **461**, 495–500 (2009).
5. N. Choi, B. Zhang, L. Zhang, M. Ittmann, L. Xin, *Cancer Cell* **21**, 253–265 (2012).
6. M. Ousset *et al.*, *Nat. Cell Biol.* **14**, 1131–1138 (2012).
7. O. J. Kwon *et al.*, *iScience* **13**, 328–338 (2019).
8. H. Vidarsson *et al.*, *PLOS ONE* **4**, e4471 (2009).
9. D. T. Montoro *et al.*, *Nature* **560**, 319–324 (2018).
10. L. W. Plasschaert *et al.*, *Nature* **560**, 377–381 (2018).
11. S. R. Blomqvist, H. Vidarsson, O. Söder, S. Enerbäck, *EMBO J.* **25**, 4131–4141 (2006).
12. O. J. Kwon, L. Zhang, L. Xin, *Stem Cells* **34**, 191–202 (2016).
13. S. Ross, S. D. Spencer, L. A. Lasky, H. Koeppen, *Am. J. Pathol.* **158**, 809–816 (2001).
14. H. F. English, R. J. Santen, J. T. Lsaacs, *Prostate* **11**, 229–242 (1987).
15. G. S. Evans, J. A. Chandler, *Prostate* **11**, 339–351 (1987).
16. A. S. Goldstein *et al.*, *Proc. Natl. Acad. Sci. U.S.A.* **105**, 20882–20887 (2008).
17. K. R. Moon *et al.*, *Nat. Biotechnol.* **37**, 1482–1492 (2019).
18. H. J. Snippert *et al.*, *Cell* **143**, 134–144 (2010).
19. A. Van Keymeulen *et al.*, *Nature* **479**, 189–193 (2011).
20. J. Liu *et al.*, *Mol. Endocrinol.* **25**, 1849–1857 (2011).
21. G. R. Cunha, B. Lung, *J. Exp. Zool.* **205**, 181–193 (1978).
22. Q. Xie *et al.*, *Nat. Commun.* **8**, 14284 (2017).
23. J. A. Ramilowski *et al.*, *Nat. Commun.* **6**, 7866 (2015).
24. P. C. Marker, A. A. Donjacour, R. Dahiya, G. R. Cunha, *Dev. Biol.* **253**, 165–174 (2003).
25. A. A. Donjacour, A. A. Thomson, G. R. Cunha, *Dev. Biol.* **261**, 39–54 (2003).
26. W. Luo *et al.*, *Stem Cells* **31**, 2492–2505 (2013).
27. V. Mehta *et al.*, *Dev. Dyn.* **240**, 2548–2560 (2011).
28. I. Tirosh *et al.*, *Science* **352**, 189–196 (2016).
29. B. S. Taylor *et al.*, *Cancer Cell* **18**, 11–22 (2010).
30. G. H. Henry *et al.*, *Cell Rep.* **25**, 3530–3542.e5 (2018).
31. E. L. Rawlins *et al.*, *Cell Stem Cell* **4**, 525–534 (2009).
32. K. U. Hong, S. D. Reynolds, A. Giangreco, C. M. Hurley, B. R. Stripp, *Am. J. Respir. Cell Mol. Biol.* **24**, 671–681 (2001).
33. J. R. Schaub, Y. Malato, C. Gormond, H. Willenbring, *Cell Rep.* **8**, 933–939 (2014).
34. Z. A. Wang *et al.*, *Nat. Cell Biol.* **15**, 274–283 (2013).
35. L. Zhu *et al.*, *Cell* **166**, 1132–1146.e7 (2016).

ACKNOWLEDGMENTS

We thank members of the Regev and Sawyers laboratories for valuable critiques and discussions; the Molecular Cytology Core Facility at MSKCC for help with confocal microscopy and IHC; and the Flow Cytometry Core Facility at MSKCC for help with FACS experiments. **Funding:** C.L.S. is supported by HHMI; National Institutes of Health grants CA193837, CA092629, CA224079, CA155169, and CA008748; and Starr Cancer Consortium grant I12-0007. A.R. is an HHMI Investigator and is supported by the Klarman Cell Observatory, NCI grants 1U24CA180922 and R33-CA202820, Koch Institute NCI Support (core) grant P30-CA14051, and the Ludwig Center at MIT (AR). W.R.K. is supported by a fellowship from the Dutch Cancer Foundation and a Prostate Cancer Foundation Young Investigator Award. **Author contributions:** W.R.K. and C.L.S. conceived the project. W.R.K. designed the experiments. W.R.K. performed staining and confocal microscopy. W.R.K., M.H., A.R., and C.L.S. wrote the manuscript. W.R.K, D.C., and E.L.L. performed all mouse work. W.R.K. performed all organoid work. M.H. and A.B. performed bioinformatics analyses. W.K., M.H., A.R., and C.L.S. interpreted the data. M.T. performed IHC and RNA FISH. B.C., A.G., and W.A. provided human prostate samples. M.B., O.C., I.M., O.C., and T.X. performed single-cell sequencing. L.M. and D.P. oversaw the single-cell–sequencing experiments. A.R. and C.L.S. oversaw the project. **Competing interests:** C.L.S. is on the board of directors of Novartis, is a cofounder of ORIC Pharmaceuticals, and is a coinventor of the prostate cancer drugs enzalutamide and apalutamide, covered by U.S. patents 7,709,517, 8,183,274, 9,126,941, 8,445,507, 8,802,689, and 9,388,159 filed by the University of California. C.L.S. is on the scientific advisory boards of the following biotechnology companies: Agios, Beigene, Blueprint, Column Group, Foghorn, Housey Pharma, Nextech, KSQ Therapeutics, Petra Pharma, and PMV Pharma, and is a cofounder of Seragon Pharmaceuticals, purchased by Genentech/Roche in 2014. A.R. is a cofounder of and equity holder of Celsius Therapeutics, equity holder of Immuntias, and is on the scientific advisory boards of Syros Pharmaceuticals, Neogene Therapeutics, ASIMOV Biotechnology, and ThermoFisher Scientific. W.R.K. is a coinventor on patent WO2012168930A2 filed by Koninklijke Nederlandse Akademie Van Wetenschappen that covers organoid technology. **Data and materials availability:** Mouse gene expression data are available at the Gene Expression Omnibus repository https://www.ncbi.nlm.nih.gov/geo/ (accession no. GSE146811). Human raw data are available at the Data Use and Oversight System controlled access repository: https://duos.broadinstitute.org/ (accession no. DUOS-000115). Processed expression data can be downloaded and explored at: https://singlecell.broadinstitute.org/single_cell/study/SCP859 (mouse data) and https://singlecell.broadinstitute.org/single_cell/study/SCP864 (human data).

SUPPLEMENTARY MATERIALS

science.sciencemag.org/content/368/6490/497/suppl/DC1
Materials and Methods
Figs. S1 to S24
Tables S1 to S9
References (*36*–*49*)

View/request a protocol for this paper from *Bio-protocol*.

15 May 2019; accepted 14 March 2020
10.1126/science.aay0267

Regenerative potential of prostate luminal cells revealed by single-cell analysis

Wouter R. Karthaus, Matan Hofree, Danielle Choi, Eliot L. Linton, Mesruh Turkekul, Alborz Bejnood, Brett Carver, Anuradha Gopalan, Wassim Abida, Vincent Laudone, Moshe Biton, Ojasvi Chaudhary, Tianhao Xu, Ignas Masilionis, Katia Manova, Linas Mazutis, Dana Pe'er, Aviv Regev and Charles L. Sawyers

Science **368** (6490), 497-505.
DOI: 10.1126/science.aay0267

Equal opportunity tissue regeneration

Tissue regeneration is thought to be driven primarily by rare stem cells with distinctive properties. Single-cell RNA sequencing allows rigorous testing of this hypothesis. Karthaus *et al.* examined the regeneration of normal prostate tissue in mice after androgen ablation, a common treatment for prostate cancer (see the Perspective by Kelly). Unexpectedly, they found that in addition to rare stem cells, a large population of differentiated cells was a major contributor to prostate regeneration, a result that they confirmed in a study of human prostate tissue. Investigation of the molecular mechanism by which the differentiated cells acquired regenerative potential yielded insights that could potentially lead to improved therapies for prostate cancer.

Science, this issue p. 497; see also p. 467